The following publication Y. -c. Shen, M. -l. Chen, Y. -p. Du and W. -s. Dong, "Line Charge Densities and Currents of Downward Negative Leaders Estimated From VHF Images and VLF Electric Fields Observed at Close Distances," in IEEE Transactions on Electromagnetic Compatibility, vol. 61, no. 5, pp. 1507-1514, Oct. 2019 is available at https://doi.org/10.1109/TEMC.2018.2864199.

Line Charge Densities and Currents of Downward Negative Leaders Estimated from VHF Images and VLF Electric Fields Observed at Close Distances

Yan-chi Shen, Ming-li Chen, Ya-ping Du and Wan-sheng Dong

***Abstract*—The channel charge distribution of a lightning leader is a critical parameter for the study of lightning mechanism. However, there is little experiment-based result on it, mainly due to lacking adequate methods for getting the leader charge distribution with ordinary ground observations. In this paper, a method for retrieving the line charge density and the current of a downward leader based on ground observations of lightning images and electric field changes was proposed and examined. The method was then applied to two downward negative leaders in a rocket-triggered lightning discharge with measurements of broadband interferometric images and electric field changes at close distance. Only the descending channel portion between about 900 to 400 m high of the two leaders were analyzed, where the channel was in free air rather than the trace of triggering wire. The line charge density for both leaders showed a general increasing trend with a big impulsive change around 500 m high, as the leaders moved downward, which was in good agreement with the prediction of existing downward leader models. The range of the line charge density was similar for the two leaders (-0.03 to -0.32 mC/m and -0.02 to -0.33 mC/m, respectively). The impulsive change of the line charge density was corresponding to a sharp turn of the leader channel around 500 m high, which may imply that the sharp turn of the leader channel was probably associated with a pre-existing local positive space charge pocket. The estimated leader current ranged from -20 A to -315 A and from -77 A to -541 A for the two leaders, respectively, which was in good agreement with independent estimations in the literature.**

***Index Terms*—Downward leader, leader speed, leader current, line charge density**

I. Introduction

A lightning stroke to a grounded object usually involves at least one downward-leader/upward-return-stroke process. Understanding the property of downward leader inception and propagation is critical to the protection of structures against lightning. However, most existing studies on downward leaders are mainly concentrated on observations of the leader spatial evolution and leader-produced VLF/VHF electromagnetic signals with cameras or electric and magnetic antennas. There is little information about the evolution of charges and currents along downward leader channels in the literature, mainly due to lack of means to measure directly these parameters. On the other side, knowing the leader charge distribution is essential for the evaluation of strength and lightning striking distance to a grounded object of the return stroke following the leader [1].

Brook et al. [2] reported that the total charge deposited on downward leader channels was in the range from a few coulombs to 10 C to 20 C. Schonland et al. [3] reported that the average charge per unit length lowered down from the cloud into leader channels was in the order of 1 mC/m. Some researchers considered that the charge density of downward leaders was uniformly distributed in a range of 0.02 to 1.4 mC/m [4]. Some researchers argued that the leader charge density should decrease with the height, because the capacitance between the leader channel and the ground is getting bigger with height [5-9].

According to remote magnetic field measurements of two leaders, Williams and Brook [10] reported that the average currents of the two leaders were 50 A and 63 A respectively. Thomson [6] reported that 62 leader currents estimated from electric field measurements had a mean value of 1.3 kA ranging from 100 A to 5 kA. Krehbiel [11] reported that the final leader currents from multiple-station electric field measurements averaged more than 1.3 kA for a few leaders.

In contrast to the limited experimental studies, there are many simulative studies of downward leaders with various models [12-16]. Although different models assumed different parameter values at certain stages of the leader process, most of these models predicted an increasing leader line charge density as the leader moves downward.

Recently, Chen et al. [17] proposed an approach to estimate the spatial and temporal evolution of the line charge density and current of upward leaders based on observations of leader

Works leading to this paper are partly supported by The Hong Kong Polytechnic University and Research Grant Council of Hong Kong Government (Grant No.: PolyU152022/14E).

Yan-chi Shen is with the School of Electrical Engineering, Nantong University, Nantong, Jiangsu, China (e-mail: shenyanchi@ntu.edu.cn).

Ming-li Chen is with the Department of Building Services Engineering, The Hong Kong Polytechnic University, HK. (e-mail: mingli.chen@polyu.edu.hk).

Ya-ping Du is with the Department of Building Services Engineering, The Hong Kong Polytechnic University, HK. (e-mail: ya-ping.du@polyu.edu.hk).

Wan-sheng Dong is with the Chinese Academy of Meteorological Sciences, Beijing, China (e-mail: dongwsh@cams.cma.gov.cn).

channel images and electric field changes at close distance. They rebuilt the leader channel in 2-dimensional way, and then applied the approach to two upward positive leaders obtained in classically rocket-triggered lightning. The estimated line charge densities and hence the currents were well consistent with the measured currents.

In this study, we propose and practice a modified method for retrieving the charge density of a downward leader from the VHF interferometer, photograph and electric field change observations of the leader. The VHF interferometer system with higher time resolutions can acquire the leader process which may not be visible from the camera image. The modified method will be then applied to two downward negative dart-leaders in triggered lightning to study their charge and current evolution, as in [17]. The modified method can be used in different types of measurements where the leader could be mapped 3-dimensionally by camera or VHF lightning mapping system. Details of the leader studied and the method application results are given in following sections.

II. Lightning Data and Leader Channel Evolution

A. Lightning data

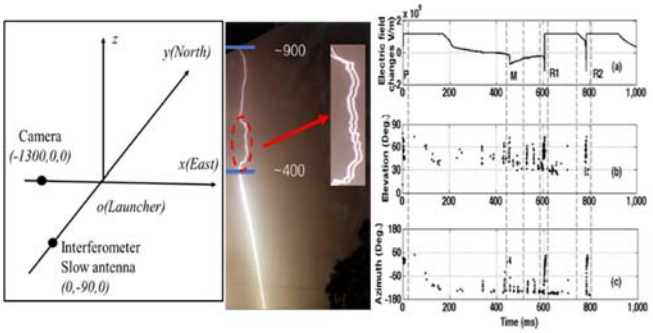

Fig. 1. The observation setup and the raw data obtained for the triggered–lightning discharge to be studied. The left panel is the observation setup and coordinates for the discharge: x-axis is from west to east, y-axis is from south to north. The middle panel is a photograph of the discharge from the camera located 1.3 km west to the launcher. The right panel is the raw data of the discharge: (a) the electric field change recorded by the slow antenna, (b) the elevation and (c) the azimuth of the VHF radiation sources located by the interferometer at 90 m south to the launcher. The azimuth from the interferometer to the launcher on y-axis is set to 0° and it increases in counterclockwise. The time 0 is referred to the triggering time of the slow antenna and the interferometer system.

The lightning leaders we analyzed here were obtained in a rocket-triggered discharge at 21:18:36 (Beijing Time) on July 10 of 1999 in Southern China. The discharge was initiated when the rocket ascended to about 400 m high (estimated from the length of the wire the rocket spouted out, which measured about 460 m long and inclined) and the ground electric field was negative before launch of the rocket. Detailed information of observation systems of that discharge can be found in Dong et al. [18]. The measurements included a camera at 1.3 km west to the launcher, a broadband interferometer (bandwidth 25~100 MHz) and a slow antenna with a time constant of 6 s (bandwidth 0.03 Hz ~1 MHz) to record the electric field changes both at 90 m south to the launcher, and a fast field change antenna with a time constant of 2 ms. During the data analysis, digital filter was used to make sure the VHF data within the bandwidth of 25~100 MHz. The frame rate of the camera was 2000/s. For the analysis, we set that the launcher position was as the origin of the (x, y, z) coordinates, the camera was on the x-axis at (-1300m, 0, 0) and the interferometer and slow antenna were on the Y-axis at (0, -90m, 0), as shown in the left panel in Fig. 1 (not drawn in scale).

The discharge included a preliminary leader process, followed by an M-component-wise process and two successive leader/return stroke processes. There might be an upward positive leader initiated from the tip of the triggering wire, which most likely occurred during the time period 0~2ms or even some time before the abrupt electric field. However, due to its faintly luminous channel and less and weaker VHF radiations, it might be simply missed by both the camera and the interferometer, since a positive leader when compared with a negative leader may not be able to trigger a lighting interferometer system. Detailed discussion of this lightning process can be found in Chen et al. [19].

Fig. 1 shows the observation setup and raw lightning data obtained for the discharge to be analyzed. The middle panel in the figure is a photograph of the discharge from the camera at 1.3 km west of the rocket launcher, which shows a single channel with a small horizontal offset between two strokes caused by wind. The lower straight part under about 400 m high in the photograph is the lightning channel with residual vaporized wire. The upper bent part between two blue bands, which is estimated to be from about 400 m to 900 m above ground, is believed to be the main channel formed by the two leader-return-strokes in air.

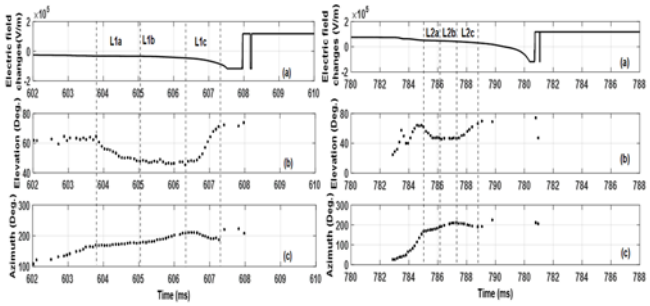

Fig. 2. Expansions of the raw lightning data in Fig.1 for the two leader-return-strokes to be studied. Left 3 panels are for the first leader-return stroke (L1/R1) and right 3 panels for the second leader-return stroke (L2/R2). L1a, L1b and L1c stand for 3 stages of the L1, and L2a, L2b and L2c stand for that of the L2. (a) The electric field change from the slow antenna, (b) the elevation and (c) the azimuth of the VHF radiation sources from the interferometer.

Fig.2 is the expansion of the raw lightning data in Fig. 1 for the two leader-return-strokes (L1/R1 and L2/R2) to be studied. As seen from the figure, the first leader (L1) (the leader before the first return stroke) lasted about 10 ms. Since the discharge was very close to the sensor, the electric field changes were partly saturated. In the time period from about 603.8 ms to 607.5 ms, the leader was characterized by a slow negative-going electric field change with many VHF sources located. In contrast to this period, after the time 607.5 ms but just before the return stroke, the leader showed a fast negative-going

electric field change with few VHF sources located. This might be probably because that the leader just before the return stroke ran downward along the conductive triggering wire trace, resulting in less and weak VHF radiations. It is generally thought that lightning currents propagating in a well conducting channel do not produce any VHF radiation [19-21]. The only three VHF sources in the just before the return stroke may be not radiated from the leader channel or they may be resulted from erroneous locations [22]. The leader period in the time period of 603.8 to 607.5 ms, which was with many VHF sources located, can be further divided into three stages, namely L1a, L1b and L1c, respectively. The elevations of VHF radiation sources showed a descending trend for L1a, a horizontally extension trend for L1b and a sharply ascending trend for L1c, while the azimuths showed a slowly ascending trend for L1a and L1b but a descending trend for L1c. Based on the analysis in [19] and the main purpose of this study, we just focus on the stage L1a, which was corresponding to the leader part moving downward from about 900m high to about 400 m high in air above the triggering wire within the view of the camera.

Similarly, as seen from Fig. 2, the second leader (L2) (the leader before the second return stroke) lasted about 5 ms. It had a similar feature to that of L1 but with a shorter propagation time. L2 can also be divided into three stages, namely L2a, L2b and L2c, respectively. The elevations showed a descending trend for L2a, a horizontally extension trend for L2b and an ascending trend for L2c, while the azimuths showed an increasing (counter clockwise) trend for L2a and L2b but a decreasing (clockwise) trend for L2c, indicating that they moved in different directions. With the same sake to L1, we just focus on L2a for further analysis.

B. Leader channel evolution in 3D

Photograph and VHF radiation sources can only provide 2D channel images of a lightning discharge respectively. To get the 3D channel and its spatial evolution for the two leaders, we have combined the photograph with the VHF radiation source data in following way. First, each point along the channel on the photograph is converted into a radial line pointing from the camera to the real lightning channel in space around the launcher. All these radial lines together will form a curved face in space (Face 1). Similarly, each pair of elevation and azimuth of the VHF source data represents a radial line that points from the interferometer to the real lightning channel in space around the launcher too. Projection of the radial lines from the interferometer onto Face 1 will give the evolution of the leader channel in 3D. Detailed discussion and the results of the lightning channel reconstruction can be found in Chen et al. [19].

Shown in Fig. 3 are (a) the rebuilt 3D channels viewed from the interferometer on x-z plane and (b) that viewed from the camera on y-z plane, (c) the channel evolution speed versus time, and (d) the electric field changes, for L1a. The red circle and mark P1 in the figure show a sharp turn of the channel there. In order to get adequate leader speed for calculating the leader charge distribution, the leader channel was divided into several large segments, each with a length no less than 100 m and a leader propagation time no less than 100 μs. Such a segmenting strategy was aimed to eliminate the influence of stepping process on the average speed estimation. The speed for L1a showed a decreasing trend from 2.34 $\times 10^6$ m/s down to 0.28 $\times 10^6$ m/s as it descended from 900 m down to 400 m high.

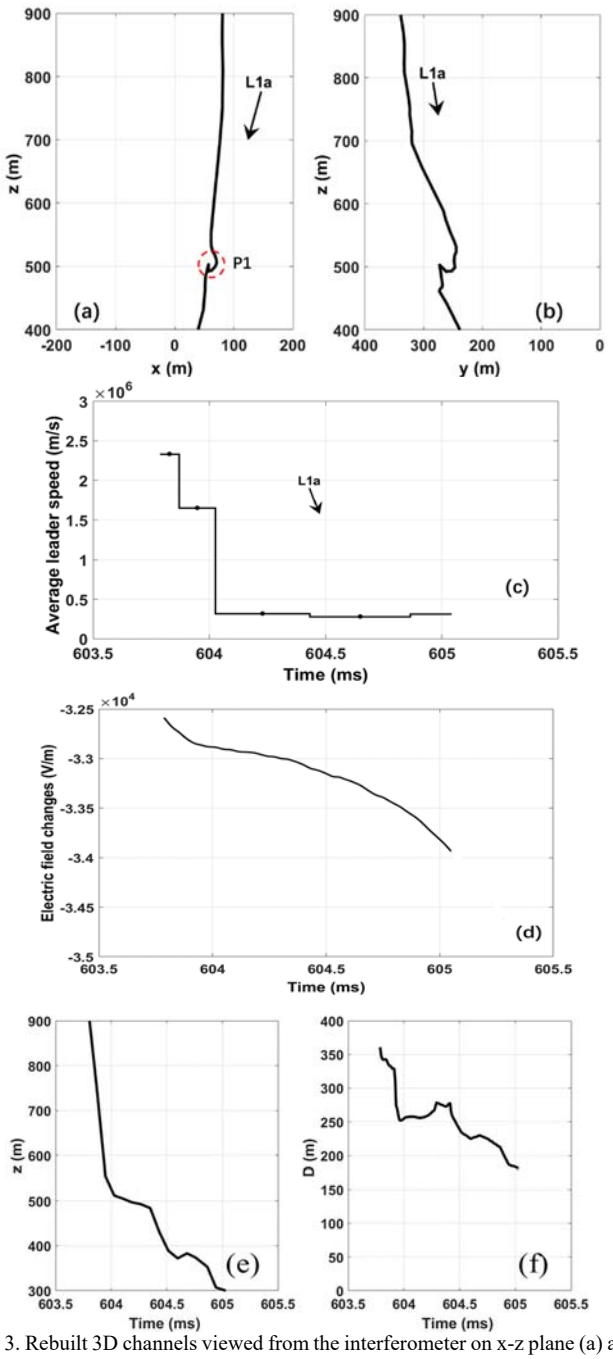

Fig. 3. Rebuilt 3D channels viewed from the interferometer on x-z plane (a) and that viewed from the camera on y-z plane (b), the channel evolution speed (c), the electric field changes (d), the leader tip height versus time (e), and the leader tip horizontal distance to the observer versus time (f), for L1a.

Similarly, Fig. 4 shows the rebuilt 3D channels viewed from the interferometer (a) and that viewed from the camera (b), the channel evolution speed (c), and the electric field changes (d), for L2a. L2a propagated downward in a similar path to L1a but with a higher speed. The red circle and mark P2 in the figure show a sharp turn of the channel there, which is similar to P1

for L1a. The speed of L2a showed also a decreasing trend from 4.12 $\times 10^6$ m/s down to 0.73 $\times 10^6$ m/s as it descended from 816 m down to 400 m high. According to the analysis in [19], the speeds of L1a and L2a were on the slow side for dart leaders. This may be due to that the time gaps between the two leader/return stroke processes as well as the preliminary leader process were too long. In literature, there is a weak statistical relationship between the lower leader speed and longer inter-leader/stroke time interval in rocket-triggered and natural lightning discharges [23].

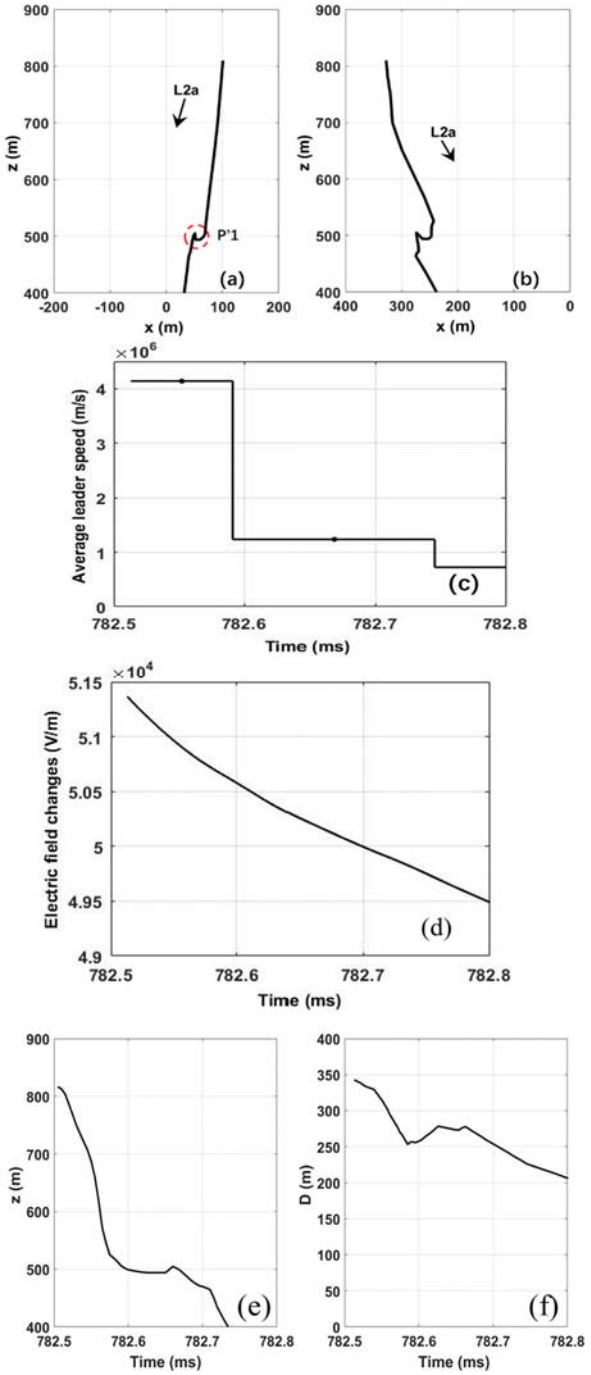

Fig. 4. Similar to Fig. 3, but for L2a: Rebuilt 3D channels viewed from the interferometer on x-z plane (a) and that viewed from the camera on y-z plane (b), the channel evolution speed (c), the electric field changes (d), the leader tip height versus time (e), and the leader tip horizontal distance to the observer versus time (f).

III. Method for Retrieving Leader Line Charge Density

A. Basic method

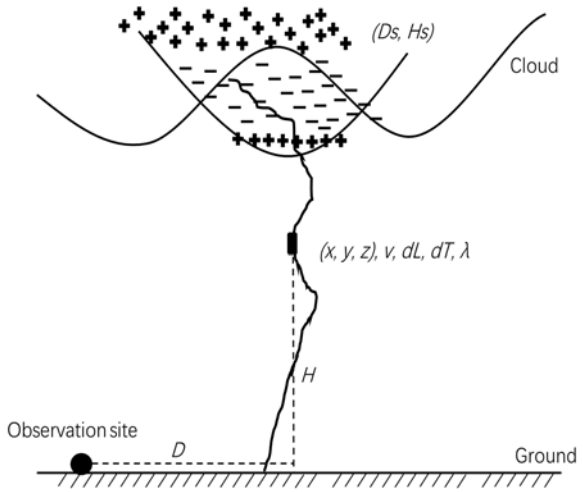

Fig. 5. A schematic diagram for illustration of a downward leader with a speed of v and line charge density of λ producing an electric field change ΔE at a distance D on ground. The image of charge has been taken into account when the electric field change calculated.

As shown in Fig. 5, suppose that a negative leader goes down from a charged cloud to the ground with a speed of $v\ (x, y, z)$ and a line charge density $\lambda\ (x, y, z)$. We assume that the charge newly added to the leader tip as the leader extends downward is directly from a negative charge source in the cloud at a height H_S and a horizontal distance D_S to an observer on ground [24, 25]. The charge deposited in the channel behind the leader tip remains unchanged as the leader goes forward. Thus, for the leader tip moves downward a tiny length of dL around a height of H and a horizontal distance of D to an observer on the ground, it will produce a vertical electric field change dE at the observer as [4, 26-29]:

$$dE = \frac{\lambda dL}{2\pi\varepsilon_0}\left(\frac{H}{(D^2+H^2)^{3/2}} - \frac{H_S}{(D_S^2+H_S^2)^{3/2}}\right), \quad (1)$$

where ε_0 is vacuum dielectric constant and $dL=vdt$ for a steadily-propagating leader moving with a speed v. Here, the image of charge has been taken into account, and the ground is perfectly conducting. The line charge density can then be expressed as a function of the leader speed and electric field change rate on the ground as:

$$\lambda = \frac{2\pi\varepsilon_0}{v}\cdot\frac{dE}{dt}\left(\frac{H}{(D^2+H^2)^{\frac{3}{2}}} - \frac{H_S}{(D_S^2+H_S^2)^{\frac{3}{2}}}\right)^{-1}. \quad (2)$$

It should be noted that Equation (2) is valid just for a tiny length of leader channel, which can be seen as point charge case.

B. Practical algorithm for estimating the leader charges

In practice, subjected to limited spatial and temporal resolutions of the observed leader channels, leader speeds and electric field changes, following algorithm may be adopted for estimating the line charge density along the leader channel:

1) To eliminate the influence of high frequency noise on the calculation of the electric field change rate, one can divide the electric field change curve into many small segments

ΔEn (n =1,…, N) in an equal time interval of Δt. Based on the slow antenna sensitivity and our testing, the value of Δt is set to 20 μs in present study. The averaged electric field change rate for each segment is then given by $\Delta En/\Delta t$.

2) Similarly, the 3D leader channel built can also be divided into many small segments ΔLn (n =1,…, N) by referring to the same time interval of Δt in segmentation of the electric field changes. Taking account of the leader speed and channel bending, each segment is supposed to have a uniform 3D speed Vn and a channel length of ΔLn starting at $l_{ns}(x_{ns}, y_{ns}, z_{ns})$ and ending at $l_{ne}(x_{ne}, y_{ne}, z_{ne})$, corresponding to a time interval of Δt starting at t_{ns} and ending at t_{ne} and an electric field change rate of $\Delta En/\Delta t$, with a uniform line charge density of λn. The electric field sensor on ground is supposed to be at $P(x_0, y_0)$.

3) For each segment, ΔLn, it can be further divided into many tiny elements ΔLn_j (j = 1,…,J) in an equal channel interval of dl ($dl = vdt = 1m$ in present study, which can be treated as a point charge case). Each element is supposed to center at l_{nj} ($x_{nj}, y_{nj}, z_{nj}, t_{nj}$), with the same segmental leader speed Vn and electric field change rate $\Delta En/\Delta t$. The line charge density for each tiny element, λn_j, can then be easily obtained by bringing the element position $l_{nj}(x_{nj}, y_{nj}, z_{nj})$, the sensor position $P(x_0, y_0)$, and the segmental leader speed Vn and electric field change rate $\Delta En/\Delta t$ into Equation (2). In general, the resulted λn_j will fluctuate significantly. This is because that the resolution of Vn and $\Delta En/\Delta t$ is at segment level, which is not matched to the element level. Such a fluctuation can be eliminated when the λn_j is integrated and averaged over a segment.

4) The line charge density for a segment (λn) can then be estimated by integrating and averaging the line charge density for each element (λn_j) in the segment. The resulted segmental line charge density (λn) in relation to the segmental leader speed (Vn) and electric field change rate ($\Delta En/\Delta t$) can be expressed by Equation (3). In general, for a time interval of 20μs, each channel segment has a length of about 10~20m, involving about 10~20 tiny elements, depending on the leader speed.

$$\lambda_n = \frac{2\pi\varepsilon_0}{V_n}\cdot\frac{\Delta E_n}{\Delta t}\left\{\frac{1}{\Delta L_n}\int_{l_{ns}}^{l_{ne}}\frac{z}{((x-x_0)^2+(y-y_0)^2+z^2)^{\frac{3}{2}}}dl - \frac{H_S}{(D_S^2+H_S^2)^{\frac{3}{2}}}\right\}^{-1}, \quad (3)$$

where, $dl = \sqrt{(dx)^2+(dy)^2+(dz)^2}$.

5) Since the charge source in the cloud is usually about 5–7 km high above the ground, it has little influence on the ground electric field change at close distance to the leader. Especially when the lower leader channel part near the ground is concerned, the second term behind minus sign of Equations (2) and (3) may be ignored.

6) The leader average current for each segment can then be estimated as:

$$I_n = \lambda_n V_n \quad (4)$$

C. *Stability testing of the proposed method*

To verify the feasibility and practicability of the proposed method, suppose that there is a leader starting at 5 km (H_S) high in cloud and going down straightly towards the ground at a uniform speed of V = 5 ×10^5 m/s. The leader has a linearly increasing line charge density with the decreasing of the height, as shown in Fig. 6. The leader has a vertical channel directly below the charge origin. The electric field change produced by the leader on the ground at a certain distance, as a function of time, can be estimated based on Equation (1). With the estimated electric field and the leader speed given, the leader line charge density as a function of height can then be retrieved based on Equation (2) for different charge source height inputs. Comparing the retrieved line charge density with the original one can show us the pros and cons of the proposed method.

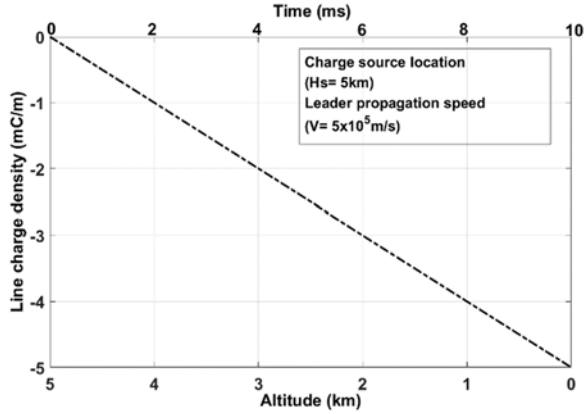

Fig. 6. The line charge density versus height for a presumed leader starting at 5 km high in the cloud and going down straightly towards the ground at a speed of 5 ×10^5 m/s.

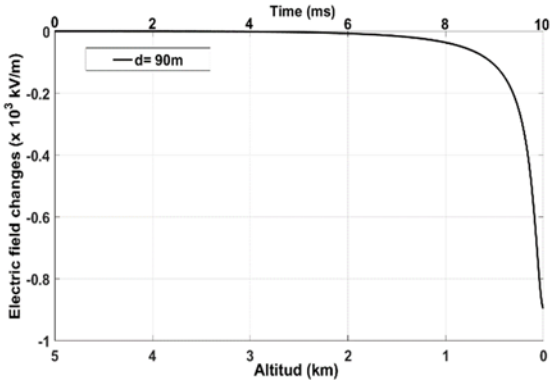

Fig. 7. Estimated ground electric field changes at 90 m away for the leader shown in Fig. 6.

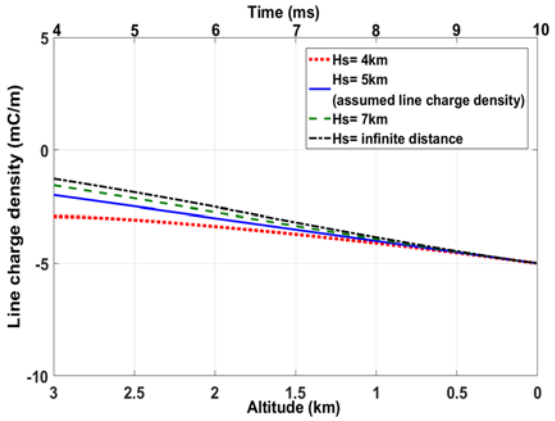

Fig. 8. The original and retrieved line charge densities with different charge source height inputs (H_S = 7 km, 5 km, 4 km and infinite, respectively), for the leader shown in Fig. 6.

To correspond to the two leaders (L1a and L2a), we assume that the electric field sensor is on the ground at 90 m away from the leader channel base. Shown in Fig. 7 are the estimated ground electric field changes at 90 m away for the leader in Fig. 6. Shown in Fig. 8 are the original and retrieved line charge densities with different charge source height inputs, for the leader in Fig. 6. Since the channels of L1a and L2a are less than 1 km high, only the results for channels below 3 km are shown in Fig. 8 for discussions.

As shown in Fig. 8, a higher charge source height input (H_S = infinity or 7 km) than 5 km leads to a larger retrieved line charge density than the original one, while a lower charge source height input (H_S = 4 km) than 5 km leads to a smaller retrieved line charge density than the original one. Nevertheless, the results for the height less than 1 km for the 3 charge source height inputs are all very close to the original charge density with the difference no more than 5%. This means that the proposed method works well when the leader channel below 1 km is concerned and the ground field change is measured at 90 m away, even if the influence of the charge source in the cloud is ignored. For a better accuracy, we suppose the charge source is at a height of H_S = 7 km for analysis of the leaders L1a and L2a in the next section.

IV. Line Charge Density Along Leader Channels

With the method in Section III and the data in Section II, the line charge density hence the leader current as a function of the channel height have been obtained for both leaders L1a and L2a. Only the channel portions between 400 m to 900 m high were concerned. As the raw data of the electric field changes are rich in high frequency noises, they are preprocessed with the five-point moving smooth method before being used for estimation of the leader line charge density. The channel is divided into many small segments each with a length ΔLn of about 10 ~ 20 m, corresponding to a time interval of about 20μs.

Shown in Fig. 9 are the line charge densities (a) and currents (b) as a function of the channel height for leader L1a, obtained based on Equations (2)-(4) with the electric field and leader channel data in Fig. 3. The red-line curve in Fig. 9 (a) is a curve-fitting of the line charge densities. The norm of residuals of the fitting curve is 0.69, indicating that the fitting curve well expresses the trend of the line charge density versus the height. The line charge densities show an increasing trend as the leader moves downward, with a big impulsive change (P1) around the height of 500 m. The range of the line charge density is from -0.026 to -0.316 mC/m. The currents, however, show a fluctuation with the height in a range of -20 to -315 A, with an obvious peak around the height of 500 m. In comparison with Fig. 3 (a), there is a sharp turn (P1) around the height of 500 m. This may imply that the sharp turn of the channel might be associated with a local space charge pocket there. As a result, it needs more charges to neutralize the local space charge when the leader tip turns to and goes through the space charge pocket area.

Shown in Fig. 10 (a) are the retrieved line charge density and (b) the current versus the channel height, based on Equations (2)-(4) and the data in Fig. 4, for the leader L2a. The norm of residuals of the fitting curve (red-line in Fig. 10 (a)) is 0.44, indicating it is a good curve-fitting of the line charge densities. The line charge densities also show an increasing trend as the leader moves downward, with a big impulsive change (P2) around the height of 500 m. The range of the line charge density is from -0.019 to -0.333 mC/m and that of the current is from -77 to -540 A.

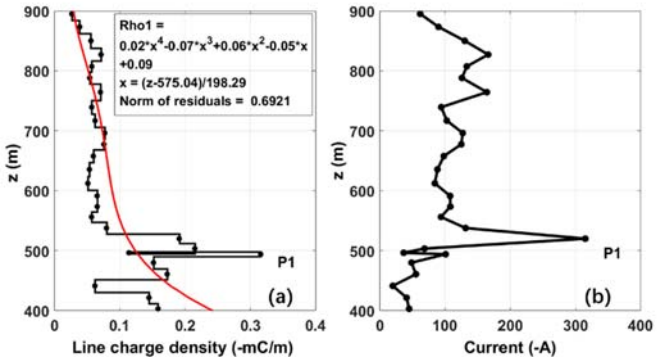

Fig. 9. The retrieved line charge density versus height (a) and the leader current versus height (b) based on the data in Fig. 3 for the leader L1a.

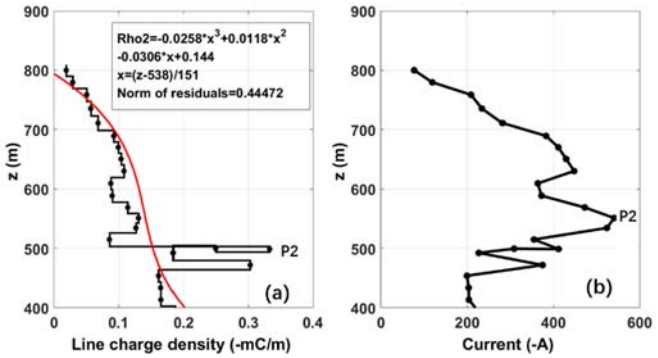

Fig. 10. Similar to Fig. 9, but based on the data in Fig. 4 for the leader L2a: (a) the line charge density versus height and (b) the leader current versus height.

V. Discussion And Conclusions

Based the data of a camera photograph, electric field changes and VHF radiation sources, the evolution of line charge density

of two downward negative leaders involved in a classically triggered discharge were investigated with a method we proposed.

Firstly, we proposed and practiced a technique for 3D channel reconstruction by combining the time-resolved VHF source data with a still photograph. Each point on the channel of the photograph can be converted into a radial line pointing from the camera to the lightning leader channel. All these radial lines together will form a curved face in space which contains the lightning leader channel. On the other side, each pair of elevation and azimuth of the VHF radiation source data also presents a radial line but pointing from the interferometer to the lightning leader channel. By projecting of the time-resolved VHF source data on to the curved face from the photograph, the 3D channel evolution of the two leaders was successfully obtained for the same lightning discharge. Limited by the camera view and the VHF sensitivity, only the channel portion between 400 m and 900 m high for the two leaders, namely L1a and L2a respectively, were analyzed. The speed of L1a decreased from about 2.34×10^6 m/s down to 2.83×10^5 m/s as it descended from 900 m down to 400 m high. The L2a also showed a decreasing trend but from 4.12×10^6 m/s down to 7.25×10^5 m/s as it descended from 900 m down to 400 m high.

Secondly, we proposed and practiced a method to retrieve the evolution of the line charge density of a leader channel based on the evolution of the 3D channel of the leader and the ground measurement of the leader-produced electric field changes. With this method and the information of the leader channel evolution and the leader-produced electric field changes, the line charge density hence the leader current as a function of the height were obtained successfully for both L1a and L2a. The line charge densities of both L1a and L2 showed a general trend of increase with the decrease of the height, with a large impulsive change appeared around the height of about 500 m. The line charge densities ranged from -0.03 to -0.32 mC/m for L1a and from -0.02 to -0.33 mC/m for L2a. The impulsive change of the line charge density seemed to be corresponding to the sharp turn of the leader channel around the height of about 500 m, which may imply that the sharp turn was probably associated with a space charge pocket there hence an impulsive leader charge transfer occurred there. In the work of Akita et al. [30], they found that the negative breakdowns changed their direction when the breakdowns reached the regions where positive charge did not exist. In other words, the charge regions can influence the direction of breakdowns. The leader current ranged from about -20 A to -315 A for L1a and from about -77 A to -541 A for L2a, which are in good agreement with independent measurements in the literature. L1 was the first leader, while L2 was the subsequent leader with lower leader initiation potential [21], which traces in the remnants of the previous L1 channel. Therefore, the fitting curves of the line charge density of these two leaders cannot be simply compared. Besides, the difference in local space charges preexisting along the leader route may also lead the difference in the line charge density between L1a and L2a.

Compared with the 2-dimentional upward positive leader channels in Chen et al. [17], the negative downward leader channels (L1a and L2a) rebuilt in 3D in this study had a larger leader speed, a similar range and trend of the line charge density with the extension of the leader, and a larger leader current. The method can be broadly used on different lightning leaders with higher observation resolutions to better understand the physical mechanism of lightning leader charge without current measurements.

REFERENCES

[1] V. Cooray, A. V. Rakov, and N. Theethayi, "The lightning striking distance—Revisited," J. Electrostatics, 65(5), 296-306, 2007.

[2] M. Brook, N. Kitagawa, and E.J. Workman, "Quantitative study of strokes and continuing currents in lightning discharges to ground," J. Geophys. Res., 67, 649–659, 1962.

[3] B. F. J. Schonland, "The lightning discharge", in Handbuch der Physik, vol. 22, edited by S. Flugge, pp. 576-628, Springer-Verlag, New York, 1956.

[4] W. H. Beasley, M.A. Uman, and P.L. Rustan "Electric fields preceding cloud to ground lightning flashes," J. Geophys. Res., 87, 4883–4902, 1982.

[5] P. F. Little, "Transmission line representation of a lightning return stroke," J. Physics D: Applied Physics, 11(13), 1893, 1978.

[6] E. M. Thomson, and M. A. Uman, "Speed and current for lightning stepped leaders near ground as determined from electric field records," J. Geophys. Res., DOI:10.1029/JD090iD05p08136, 1985.

[7] V. Mazur, L. H. Ruhnke "Model of electric charges in thunderstorms and associated lightning," J. Geophys. Res., 103:23299-23308, 1998.

[8] Y. Xu, and M. Chen, "A 3D self-organized leader propagation model and its engineering approximation for lightning protection analysis," IEEE Trans. Power Del., 28, no.4. DOI:10.1109/TPWRD.2013.2263846, 2013.

[9] V. Cooray, "Potential of a Cloud and Its Relationship to Charge Distribution on Stepped Leader and Dart Leader Channels. In: An Introduction to Lightning. Springer, Dordrecht, 2015.

[10] D. P. Williams, and M. Brook, "Magnetic measurements of thunderstorm currents: 1. Continuing currents in lightning," J. Geophys. Res., 68(10), 3243-3247, 1963.

[11] P. R. Krehbiel, "An analysis of the electric field change produced by lightning," PhD thesis, University of Manchester Institute of Science and Technology, 1981.

[12] M. Chen, X. Gou, and Y. Du, "The effect of ground altitude on lightning striking distance based on a bi-directional leader model," Atmos. Res., 125, 76-83, DOI:10.1016/j.atmosres.2012.08.019, 2013

[13] R. Klingbeil, and D.A. Tidman, "Theory and computer model of the lightning stepped leader," J. Geophys. Res., 79(6), 865-869, 1974.

[14] E. R. Mansell, D. R. MacGorman, C. L. Ziegler, and J. M. Straka, " Simulated three‐dimensional branched lightning in a numerical thunderstorm model," J. Geophys. Res.: Atmos., 107(D9), 2002.

[15] S. Tao, Y. Tan, B. Zhu, M. Ma, and W. Lu, "Fine-resolution simulation of cloud-to-ground lightning and thundercloud charge transfer," Atmos. Res., 91(2), 360-370, 2009.

[16] M. Vargas, and H. Torres, "On the development of a lightning leader model for tortuous or branched channels–Part I: Model description," J. Electrostatics, 66(9), 482-488, 2008.

[17] M. Chen, D. Zheng, Y. Du, and Y. Zhang, "Evolution of line charge density of steadily-developing upward positive leaders in triggered lightning," J. Geophys. Res. Atmos., 118, 4670–4678, DOI:10.1002/jgrd.50446, 2013.

[18] W. Dong, X. Liu, Y. Yu, and Y. Zhang, "Broadband interferometer observations of a triggered lightning," Chin. Sci. Bull., 46, No.18, 1561-1565, 2001.

[19] M. Chen, Y. Shen, Y. Du, and W. Dong, "Fine spatial evolution of leaders and M-components in rocket-triggered lightning observed with a broadband interferometer," J. Atmos. Sol. Terr. Phy., 2017.

[20] T. O. Ushio, Z. I. Kawasaki, Y. Ohta, et al., "Broad band interferometric measurement of rocket triggered lightning in Japan", Geophys. Res. Lett., 24(22):2769-2772, 1997.

[21] Z. Sun, X. Qie, R. Jiang, et al., "Characteristics of a rocket-triggered lightning flash with large stroke number and the associated leader propagation," J. Geophys. Res. Atmos., 119(23):13,388-13,399, 2015.

[22] S. Yoshida, C. J. Biagi, V. A. Rakov, et al., “Three‐dimensional imaging of upward positive leaders in triggered lightning using VHF broadband digital interferometers”, Geophys. Res. Lett., 37(5):137-147, 2010.
[23] D. M. Jordan, V. P. Idone, V. A. Rakov, et al., “Observed dart leader speed in natural and triggered lightning”, J. Geophys. Res. Atmos., 97(D9):9951-9957, 1992.
[24] P. Lalande, A. Bondiou-Clergerie, P. Laroche, A. Eybert-Berard, J. P. Berlandis, and B. Bador, B., et al. “Connection to ground of an artificially triggered negative downward stepped leader”, Proc. 10th International Conference on Atmospheric Electricity, Osaka, Japan, 1996.
[25] M. Becerra, and V. Cooray, “Time dependent evaluation of the lightning upward connecting leader inception”. J. Phys. D: Appl. Phys, 39, 4695–4702, 2006.
[26] E. M. Thomson, "A theoretical study of electrostatic field wave shapes from lightning leaders." J. Geophys. Res. Atmos. 90. D5 :8125-8135, 1985.
[27] V. Mazur and L. H. Ruhnke. "Determining leader potential in cloud to ground flashes." Geophys. Res. Lett. 29.12:42-41,2002.
[28] D. J. Malan and B. F. J. Schonland, “Progressive lightning; directly-correlated photographic and electrical studies of lightning from near thunderstorms”, Proc. Roy. Soc. London, A 191(1027), 485-503, 1947.
[29] M. A, Uman, “Lightning”, pp.54, 211-214, McGraw-Hill, New York, 1969
[30] M. Akita, T. Morimoto, T. Ushio, et al. “The relationship between the leader progressions and the charge distributions”. Ursi Radio Science Bulletin, No. 377, 2011

Line Charge Densities and Currents of Downward Negative Leaders Estimated From VHF Images and VLF Electric Fields Observed at Close Distances

August 2018

IEEE Trans. on Electromagnetic Compatibility
PP (99):1-8, DOI: 10.1109/TEMC.2018.2864199